A 3-Phase Solver for the Simulation of Internal Nozzle Cavitating Flows in Fuel-Injectors using OpenFOAM

F. Giussani[1], F. Piscaglia[1,*], J. Hélie[2], S.M. Aithal[3]
[2]Continental Automotive SAS, France
[3]Argonne National Laboratory, Lemont, USA
[1]Dept. of Aerospace Science and Technology (DAER), Politecnico di Milano, Italy

*Corresponding author: federico.piscaglia@polimi.it

Abstract
A novel multiphase Volume-of-Fluid (VOF) solver to model the physics of the internal nozzle flow and primary jet breakup in high-pressure injection is presented. The solver includes extensions to cavitation modeling to support phase change in presence of three phases (fuel-vapor, fuel-liquid and non-condensable gases), that are tracked in a single-fluid framework. It is shown that the tracking of the air/vapor interface is able to capture phenomena such as the hydraulic flip and the string cavitation. Code validation is carried out on two transparent glass nozzle geometries for detailed comparison of experiments and high-fidelity LES simulations. Data analysis is performed to understand how the vorticity dynamics is linked to the cavitation and atomization process to find a correlation with the vapor production. The proposed approach favors an accurate track of the evolution of the different phases within the nozzle hole and a very detailed description of the vortex generation in the injector nozzle, in presence of primary atomization of the jet. Moreover, the implemented phase-change model is able to predict how vorticity and cavitation develops within the nozzle and their influence on the atomization process. The developed code is included in a C++ Object-Oriented Library developed by the authors at PoliMi/DAER, that is linked to the most recent releases of OpenFOAM.

Keywords
Internal nozzle flows, VOF-LES, cavitation, primary breakup, multiphase flows, OpenFOAM, LibPoliMi/DAER

Introduction
Cavitation modeling in high-pressure injection involves the simulation of multiphase (in the context of this paper refers to liquid and gas) and multicomponent (several instances of the same phase) flows. Two approaches are commonly used for the simulation of multiphase and multicomponent flows. In the first approach, each phase and/or component is considered to occupy a distinct volume and the interfaces between the phases and/or components are tracked explicitly. This approach is a generalization of two-fluid approach [1]; In the second approach, the phases and/or components are spatially averaged to lead to a homogeneous mixture; relative velocity among the phases is neglected, which implies the absence of closure for the transfer of mass, momentum and energy at the interfaces while thermal equilibrium among the different phases is usually assumed. These approach is generally identified by the Volume of Fluid (VOF) [2], the Level Set (LS) [3] and the Coupled Level Set-Volume of Fluid (CLSVOF) [4, 5, 6]. Fluid properties, such as density and viscosity, sharply vary across the interface of the different phases. Several attempts have been done to combine the potentiality of the VOF with the simplicity of mixture model. In [7] the cavitating fluid mixture (liquid and vapor) is considered as primary phase while the non-condensable gas is the secondary phase; . In [8], a mass transfer model published in [9] was extended to an eight-equation two fluid-model to include non-condensable gases. Other methods to describe a three-phase flow while considering non-condensable gases are the use of the homogeneous mixture model combined with a barotropic two-fluid cavitation model [10], or the coupling of a two-fluid approach with VOF [11]. In the latter case, a two-fluid approach is used to describe the interaction between liquid and vapor in the nozzle, while VOF is used to model the jet formation. All the mentioned models have in common the aspect that they track a single interface between the non-condensable gases and a multi-component mixture [12, 13]. Barotropic models are widely used for complex simulations because they are simple to implement and numerically stable. On the other hand, one of the main limitations using a barotropic equation of state is in the underestimation of the vorticity change due to the impossibility of taking into account the misalignment of the gradient of pressure from gradient of density $(\nabla\rho \times \nabla p)/\rho^2$ [14], unless a non-linear correlation between pressure and density is used [12]. This contribution, called baroclinity, is either important in compressible fluids but also in incompressible and inhomogeneous fluids, situation that can be identified by the interface in a VOF method. Another challenge in modeling cavitation using barotropic models is the definition of an appropriate equation of state for the mixture, which includes air in addition to liquid and vapor. Tracking the interface between coexisting miscible phases (fuel vapor and non-condensable gases in this work) in injector nozzles may be important in presence of swirl cavitation and hydraulic flip regime [15, 16], when a severe detachment of flow pockets [16, 17] transported away from the hole allows non-condensable gases to flow back into the nozzle. This happens both in simplified, straight, central hole injectors [18] and in non-axial nozzles, in which large pressure fluctuations are observed in the nozzle. Recently, attempts to extend VOF, in order to include air in transport and in cavitation model have been done [19], [20] where each phase is considered as a compressible fluid but the cavitation model used [21], [22] have been previously developed under incompressible formulation. Conversely, in work of Yuan et

al. [23], each phase is considered incompressible and isothermal but the change of density is addressed at the interface and keeps in consideration the presence of the air inside cavitation model. A multi-fluid quasi-VOF model with the transport of three phases has been proposed also in [24], considering different velocities among phases and thus momentum transfer rate among interfaces. The objective of this study is to present the development of a three phase VOF solver for three incompressible fluids (liquid fuel, fuel vapor and non-condensable gases), two of which are miscible, where fuel cavitation/condensation is modeled through the Rayleigh-Plesset equation. Code implementation has been carried out by the authors and included in a C++ library in the OpenFOAM Technology developed at PoliMi/DAER. The paper is outlined as follows: A brief description of the developped three phase solver with phase change is discussed in The first Section. Afterwards, the simulations of a three-dimensional internal nozzle flow on two configurations of glass nozzles are presented. Finally, main conclusions are summarized.

Numerical Approach

The discretization of the governing equations used in this study is based on the finite-volume approach as implemented in OpenFOAM [25]. Mass and momentum are solved using the pressure-implicit split-operator (PISO) algorithm [26]. The cavitation and the condensation term have been included in a semi-implicit formulation of the phase-fraction equations, where a flux corrected transport technique [27] is used to preserve boundedness of the solution;Turbulence is modelled using LES: large turbulent scales are resolved, while smaller scales are modeled [28, 29, 30]. This separation of scales is explicitly or implicitly [31, 32] obtained by filtering out the small flow scales that cannot be properly represented by the mesh [28]; their effect must be modeled on the filtered field by means of the so called subgrid-scale (SGS) model. Although the multiphase nature of the problem, the usage of single-phase LES models is also very popular in multi-phase simulations with one fluid-approach [33, 34, 35, 36, 37, 38]. It is worth mentioning that everal numerical studies have been led with Unsteady Reynolds Averaged Naviers Stokes (URANS) equations but this approximation can significantly underestimate the formation and the extent of cavitation due to an overestimated turbulent viscosity in the cavitating zones [39, 40, 41, 42, 43]. In particular for the following study, the turbulent viscosity μ_t is modeled using the wall-adapting local eddy-viscosity model (WALE) [44], which has been proved to be suitable for wall-bounded flows and single-fluid approach [45].

Multiphase modeling

The three-phase flow is modeled using the VOF interface capturing method [46], where the cavitating fluid, the vapor and the non-condensable gas are represented by a single-fluid approach as a mixture of phases in which the phase-fraction distribution includes a sharp yet resolved transition between the phases. Each phase i has a partial volume V_i, that is a fraction of the volume V of the cell element ($V_i \subseteq V$) and it is defined by its local volume fraction $\alpha_i \in$ [0;1]: $\alpha_i = V_i/V$, with:

$$\sum_{i=1}^{3} \alpha_i = 1 \tag{1}$$

To reduce the computational cost, in the VOF approach the fluid is treated as a mixture having a single velocity $\mathbf{U}$, a "mixture" density $\rho = \sum_i \alpha_i \rho_i$ and a mixture viscosity $\mu = \sum_i \alpha_i \mu_i$. It is important to note that density in the solver varies with pressure, through the phase transport equations. The effect of the heat transfer on the temperature, that should be accounted by solving the energy equation, is not considered in the present work. The complete system of equations for three-phase flow with phase change are the phase-fraction equations, that are written as:

$$\begin{cases} \dfrac{\partial \alpha_l}{\partial t} + \nabla \cdot (\alpha_l(\mathbf{U} - \mathbf{U}_b)) + \underbrace{\nabla \cdot (\alpha_l \alpha_v \mathbf{U}_{c_{lv}}) + \nabla \cdot (\alpha_l \alpha_{nc} \mathbf{U}_{c_{lnc}})}_{\text{compression term, liquid-vapor + liquid-noncondensable gas}} = -\dfrac{S_\alpha}{\rho_l} \\ \dfrac{\partial \alpha_v}{\partial t} + \nabla \cdot (\alpha_v(\mathbf{U} - \mathbf{U}_b)) + \underbrace{\nabla \cdot (\alpha_l \alpha_v \mathbf{U}_{c_{lv}})}_{\text{compression term, liquid-vapor}} = \dfrac{S_\alpha}{\rho_v} \\ \dfrac{\partial \alpha_{nc}}{\partial t} + \nabla \cdot (\alpha_{nc}(\mathbf{U} - \mathbf{U}_b)) + \underbrace{\nabla \cdot (\alpha_l \alpha_{nc} \mathbf{U}_{c_{lnc}})}_{\text{compression term, liquid-noncondensable gas}} = 0 \end{cases} \tag{2}$$

In the system of equations (2), S_α is a source term to model the phase-change (cavitation or condensation) at the liquid interface through the cavitation model and couples the effects of the cavitation with the evolution of the interface directly:

$$S_\alpha = \frac{\rho_v \rho_l}{\rho + \alpha_{nc}(\rho_l - \rho_{nc})} \frac{D\alpha_v}{Dt} \tag{3}$$

The subscripts *l* and *v* are adopted for liquid and vapor (that are involved in the phase change) respectively, while the subscript *nc* is adopted for non-condensable gases. It is important to note that the closure of the system of equations (2) in presence of a cavitation/condensation source term S_α requires to explicitly resolve the transport of third phase fraction (non-condensable phase), to include a cavitation model and to couple the equations with the compatibility condition (1); in this way, the system is closed and implicitly bounded, thanks to (1). In absence of source terms, 3-phase VOF solvers usually calculate the void fraction of non-condensable gases directly from

Eq. (1), that is sufficient for closure only in that case. The term $\frac{D\alpha_v}{Dt}$ in Eqs. (3) includes the effects of the phase change (cavitation/condensation) and it is therefore linked to the cavitation/condensation model. To ensure stability of the segregated solver with strong variation of the density between the phases occurring with cavitation and condensation, the continuity equation is used in its non-conservative form as suggested in [47] and which it has already been used [22, 48, 23]:

$$\nabla \cdot \mathbf{U} = -\frac{1}{\rho}\frac{D\rho}{Dt} \tag{4}$$

The advantage of using volume fluxes rather than mass fluxes (conservative form) consists of having continuous volume fluxes at the interface, thus favoring the solution of pressure correction equation. With phase change and three phases, Eq. (4) can be rewritten as:

$$\nabla \cdot \mathbf{U} = \frac{\rho_l - \rho_v}{\rho + \alpha_{nc}(\rho_l - \rho_{nc})}\frac{D\alpha_v}{Dt} \tag{5}$$

Addittionaly, Since in the FV framework, numerical diffusion “smears” the sharp liquid-gas inter-phase. In OpenFOAM, the strategy commonly followed in multiphase VOF solvers to model the transport of the void fraction consists of an add convection-based term which compresses the interface and preserves boundedness: this is similar to what is done for the treatment of the scalar-flux second-moment closure, used for the “counter-gradient” transport in some complex combustion models describing the dynamic of turbulent flames [49]. A common practice is to use the compression term only where surface sharpness wants to be preserved: in the proposed formulation, the convection-based term is used only to compress the interface between the immiscible (liquid fuel) and the miscible phases (fuel vapor and non-condensable gases), as shown in Eqs. 2. In the VOF treatment, a common closure used for counter-gradient transport has the form:

$$\nabla \cdot [\mathbf{U}_c\, \alpha\, (1-\alpha)] \tag{6}$$

where $\mathbf{U}_c$ is the compression velocity at the interface between the phases, which is a consequence of the different densities and the term $\alpha(1-\alpha)$ ensures boundedness [27]. In the VOF solver developed,the employed formulation of the compression velocity is:

$$\mathbf{U}_c = \min\left[c_\alpha |\mathbf{U}|, \max(|\mathbf{U}|)\right] \hat{\mathbf{n}}_{ij} \tag{7}$$

The compression rate should be set in order to ensure interface sharpness. Higher values of the compression rate might introduce numerical instability or slow convergence. c_α is the compression coefficient. In practical cases, $1 \leqslant c_\alpha \leqslant 4$ is a good compromise to maintain a sharp interface in complex flows including, for instance, the breakup of the liquid-jet; in most applications, it is suggested a c_α of the order of unity [27]. To ensure that the compression term does not bias the solution, it should only introduce flow of α normal to the interface in the direction of the volume average interface normal $\hat{\mathbf{n}}_{ij}$. For a three-phase solver it has been computed as net gradient of the phase $i-th$ at the interface [25]:

$$\hat{\mathbf{n}}_{ij} = \frac{\alpha_j \nabla\alpha_i - \alpha_i \nabla\alpha_j}{||\alpha_j \nabla\alpha_i - \alpha_i \nabla\alpha_j||} \tag{8}$$

In the convention adopted, $\hat{\mathbf{n}}_{ij}$ always points towards the miscible couple of fluids.
The mixture velocity is obtained by the numerical solution of the momentum equation, which under single fuid approach reads:

$$\frac{\partial(\rho\mathbf{U})}{\partial t} + \nabla\cdot(\rho(\mathbf{U}-\mathbf{U}_b)\otimes\mathbf{U}) = -\nabla\hat{p} + \nabla\cdot\boldsymbol{\tau} + \mathbf{f}_\sigma + S_U - \mathbf{g}\cdot\mathbf{x}\nabla\rho \tag{9}$$

where $\hat{p}$ is a modified pressure, $\boldsymbol{\tau}$ is the stress tensor, S_U includes the source terms, $\mathbf{f}_\sigma$ is the surface force per unit inter-facial area calculated at the fluid interface in the control volume, $\mathbf{g}$ is the gravitational acceleration. The term $-\mathbf{g}\cdot\mathbf{x}\nabla\rho$ in the RHS of Eq. (9) is a consequence of the use of the modified pressure $\hat{p}$, obtained by removing the hydro- static pressure from the static pressure: In addition to the advantage of a simpler specification of the pressure boundary condition, the use of the modifed pressure in the RHS of the momentum equation improves the numerical efficiency in the treatment of the density jump at the sharp interface. In Eq. (9), $\mathbf{f}_\sigma$ is defined as:

$$\mathbf{f}_\sigma = \sigma\,\kappa\,\hat{\mathbf{n}}\,\delta\,(\mathbf{x}-\mathbf{x_s}) \tag{10}$$

where σ is the fluid surface tension coefficient in [N/m], $\hat{\mathbf{n}}$ is the unit vector normal to the liquid interface, whose center is located in $\mathbf{x}_s$, δ is the Dirac function to ensure that the force is applied only at the liquid interface, κ is the interface curvature $[m^{-1}]$, which is defined as $\kappa \equiv \nabla\cdot\hat{\mathbf{n}}$. In Eq. (10), $\mathbf{f}_\sigma$ is always oriented towards the concave interface. It is important to note that the interface curvature used in Eq. (10) is the one of the interface of the phase with highest density (liquid in this case):

$$\hat{\mathbf{n}} = \frac{\nabla\alpha_l}{\|\nabla\alpha_l\|} \tag{11}$$

The surface tension coefficient σ appearing in Eq. (10), has been written as an average of the surface tensions weighted with the phase-fractions computed in the control volume:

$$\sigma = \frac{\alpha_v \sigma_{lv} + \alpha_{nc} \sigma_{lnc}}{\alpha_v + \alpha_{nc}} \tag{12}$$

where σ_{lv} is the surface tension between the liquid fuel and fuel vapor, while σ_{lnc} is the surface tension between liquid fuel and non-condensable gases. Finally, to compute the surface tension force, the term $\hat{\mathbf{n}}\,\delta\left(\mathbf{x} - \mathbf{x}_s\right)$ in Eq. (10) must be also modeled. The Continuous Surface Force (CSF) approximation [50] is therefore used, yielding to the final form $\mathbf{f}_\sigma = \sigma\kappa\nabla\alpha_l$.

Cavitation model

Cavitation may consist either of small bubbles (bubbly-flow cavitation) or may contain large pockets of vapor (cloud cavitation) [51]; with a sharp interface-capture method, the bubble must be larger than the cell to be accurately resolved, otherwise a sub-model is needed. In the approach followed in this work, a sub-model for cavitation is always used to provide an expression for the term $\frac{D\alpha_v}{Dt}$, for the closure of the system of governing equations (2), (5) and (9).

The rates of fuel vaporization and condensation are determined by a simplification of the Rayleigh-Plesset equation which assumes spherical bubbles of radius R subject to uniform pressure variations. Spherical bubbles are then represented by a fraction of the vapor phase in the computational cell; from [48] and considering that liquid, vapor and non-condensable gases may coexist in a control volume, it follows:

$$V_v = N_b \frac{4}{3}\pi R^3 = n_0 * V_l * \frac{4}{3}\pi R^3 \tag{13}$$

where V_v and V_l are respectively the volume of the vapor and the liquid in the computational cell of volume V, N_b is the number of spherical bubbles of radius R in the computational cell and n_0 is defined as the bubble concentration per unit volume of pure liquid.

Test cases

It can be noticed the presence of the term $(\mathbf{U} - \mathbf{U}_b)$ in Eq. 2 and in Eq. 9 represents the relative velocity field between the fluid and the moving boundary. The term has been put to underline that the solver is able to handle moving boundaries problem through topological changing grids as already used by the authors [52]. However in the present work the test cases have domains which do not undergo modification in time, thus $\mathbf{U}_b$ is zero. [53].

Glass nozzles

Simulations have been performed on two different glass nozzle injectors provided by Continental, whose geometrical features are shown in Tab, 1. The simulated domain is made up of the 2 geometries shown in Fig. 1 coupled with a cylindrical chamber of $3\,\mathrm{mm}$ length and $1.5\,\mathrm{mm}$ diameter representing the injection chamber, where spray pattern analysis have been performed.

Table 1. Nominal Geometrical features of configuration 3 and 10 of the glass nozzles

Geometry $[\mu\mathrm{m}]$	Reconstructed Config. 3	Reconstructed Config. 10
Nozzle Length (L)	351	238
Sac Height (H)	134	104
Inlet Diameter (D_{in})	169	169.9
Outlet Diameter (D_{out})	145.8	153.1
Lift	81	85
Off h	104	101.98
Dead space lenght	135.7	137.2
K $\left(\frac{D_{in} - D_{out}}{D_{out}}\right) \cdot 100$	15.91 %	10.97 %

The n-Heptane is used in the experiments at feeding pressure of 100 bar. It is injected in a reservoir fill with air in quiescient state. The thermodynamic conditions of the fluids are listed in Tab. 2. The cases are intialised filling the top part of domain with liquid n-Heptane and the bottom chamber with air. A ramp on pressure from 0 to 100 bar is given at the inlet within a window of time of 5 μs. After the fields have reached statistical convergence, which happens at approximatley 0.15 ms, run time average has been performed, till 0.25 ms to have information on the mean flow.

These two configurations has been chosen, since they represents respectively Best of The Best (conf.3) and Worst of The Worst (conf10) in terms of Jet Wise Penetration (JWP). In Fig. 2 can be noticed how, this difference of JWP is strictly correlated to different geometrical features which in the end lead to different internal nozzle flow and thus to different primary jet atomization. Close-up views of the spray have been performed for both the configuration

using high-speed velocity cameras; measurements have been performed on two different direction, front view and side view.

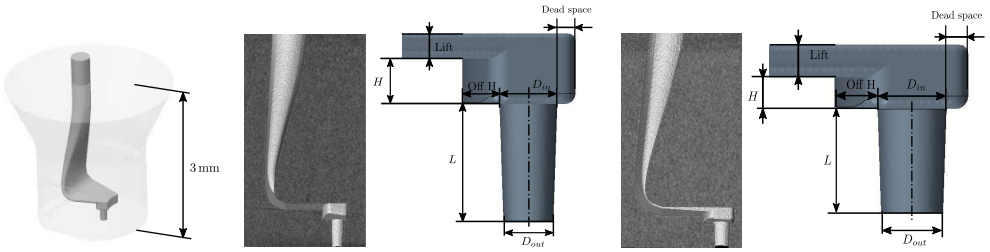

(a) feeding system (b) Config. 3 (c) Config. 10

Figure 1. (a) Geometry of the feeding system, (b) Configuration 3, (c) Configuration 10

Table 2. Thermodynamic properties for $\mathrm{n-Heptane_{(liq)}}$, $\mathrm{n-Heptane_{(vap)}}$, and non-condensable gas (air) at T=20° C.

Parameter	Fluid			Unit
	$\mathrm{n-Heptane_{(liq)}}$	$\mathrm{n-Heptane_{(vap)}}$	air	
density	684	4.25	1.225	$\mathrm{Kg/m^3}$
dynamic viscosity	$4.0835 \cdot 10^{-4}$	$7.0125 \cdot 10^{-6}$	$1.7885 \cdot 10^{-5}$	$\mathrm{Kg/(ms)}$
surface tension	0.019517			N/m
saturation pressure	7000			Pa

The configuration 3, which has the highest step and the longest nozzle, tends to produce less vapour than the shortest configuration (conf. 10). This is denoted by blue iso-surface inside the nozzle: The longer the step/Nozzle the more the vapour will reach the nozzle outlet section.

(a) $t = 0.15$ ms (b) $t = 0.17$ ms (c) $t = 0.19$ ms (d) $t = 0.21$ ms (e) $t = 0.23$ ms (f) $t = 0.25$ ms

Figure 2. Configuration 3 in the top row, Configuration 10 in the bottom row. From (b) to (g) evolution of the spray from nozzle flow to spray primary breakup. Blue, light-blue and grey surfaces denote respectively vapour-liquid interface inside the nozzle (iso-value $\alpha_l = 0.5$), vapour-liquid interface outside nozzle (iso-value $\alpha_v = 0.5$), liquid-air interface (iso-value $\alpha_{nc} = 0.5$).

On the contrary, light-blue isosurface denotes both the vapour which is produced outside the nozzle due to local pressure drops for a sudden expansion of the jet in the chamber, either part of the vapour produced in the nozzle which is leaving the injector. In both cases it stays within the core of the jet. Finally, the grey isosurface denotes the liquid-air interface, representative of the jet atomization. The time average spray, obtained by the numerical simulations, has been compared with the time average spray from experimental measurements. The compariosn is shown in Fig. 3.

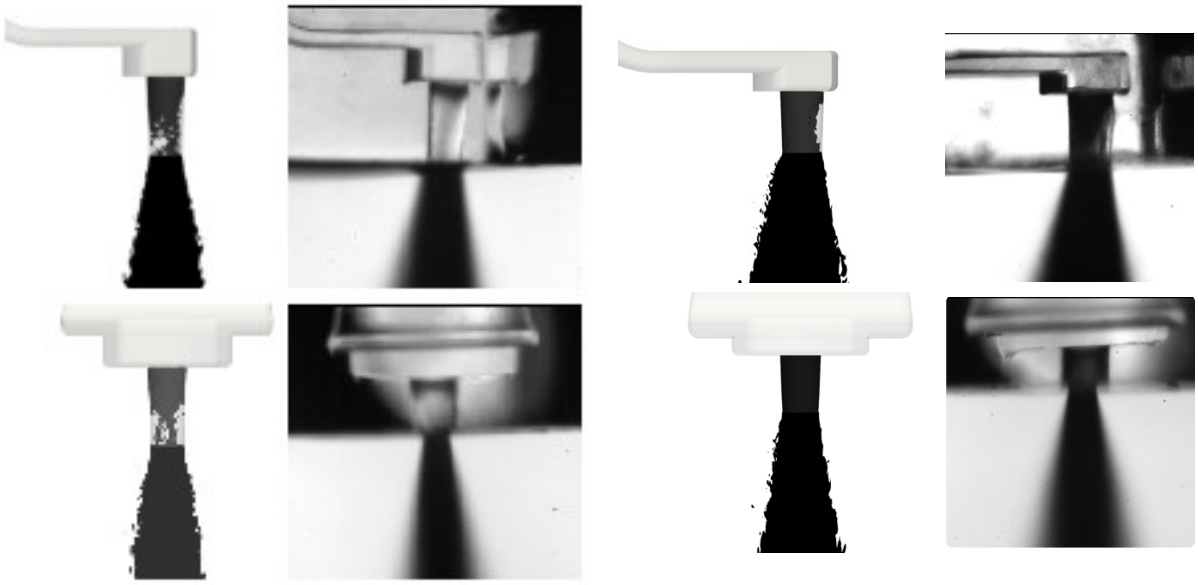

(a) Config. 3 (b) Config. 10

Figure 3. Comparison of Experimental average spray and numerical average spray. Side view on the top row, Front view on the bottom row: (a) Configuration 3, on the left numerical results, on the right experimental results.(b) Configuration 10, on the left numerical results, on the right experimental results

For both the configurations, average spray angle is well described. It must be underlined that in the front view, the light source, use for the measurements, when impacts on the curved part of the glass nozzle, tends to distord the images recorded by the camera, affecting the real proportion of the geometries.
The time average liquid field in Fig .4 shows that mean behaviour of the Config. 3 (Fig, 4-(a)) is completely different from mean beahviour of Config. 10 (Fig, 4-(b)). The former has no more vapour at half of nozzle legth, while the latter has vapour reaching the nozzle outlet section.

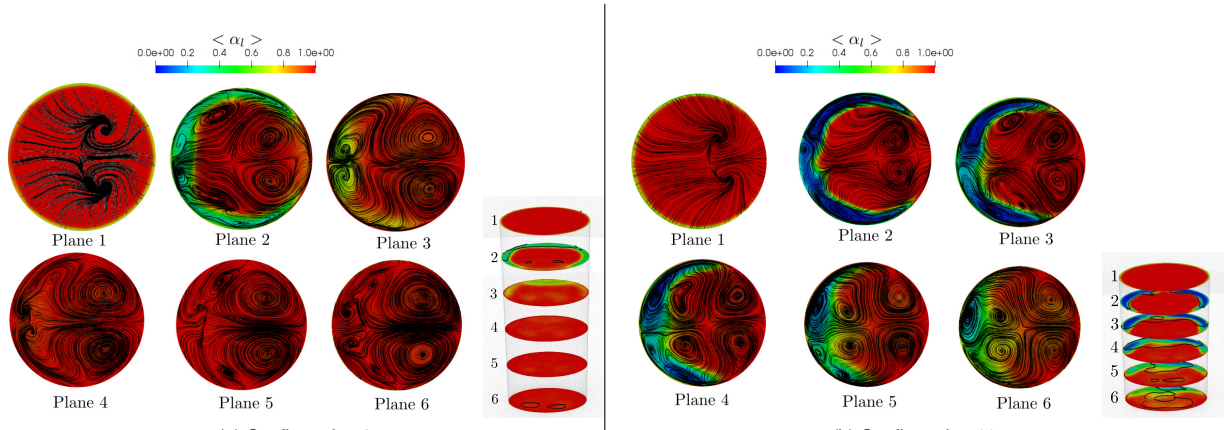

(a) Configuration 3 (b) Configuration 10

Figure 4. Nozzle cutting plane view: (a) On the left, Averaged liquid volume fraction with averaged streamlines of Config. 3. On the right, Averaged liquid volume fraction with averaged Pressure contour at p_{sat}. (b) On the left, Averaged liquid volume fraction with averaged streamlines of Config. 10. On the right, Averaged liquid volume fraction with averaged Pressure contour at p_{sat}

Average velocity streamlines on the planes, clearly indicate the presence of counter rotating streamwise vortices: Two big structures can be indentified in both the geometries at right side of cutting plane. Other smaller structures are more visible in the Configuration 10, while they seem to be smaller and confined towards the left side in the Configuration 3. The left side structures are responsible for pressure drops along streamwise direction leading to string cavitation. However, from average field on the right of Fig. 4, average pressure contour at p_{sat} value shows that the probability to find most of the times the string in the nozzle is lower than having the cavitation due to the step at the entrance of the nozzle. This mean that the string cavitation is a periodic phenomena which surely influence the atomization process but can be classified as the second responsible. Most of the cavitation comes from the fact that fluid vena is detached at the entrance of nozzle, leading to a local pressure drop, triggering the cavitation. Nevertheless, can be evinced that string cavitation is present and occurs much more in configuration 10. The iso-

surfaces of $\lambda 2$ criterion, inside the nozzle, shown in Fig. 5 (Config. 3) and Fig. 6 (Config. 10), confirm the presence of two big main structures on the right side of the nozzle. $\lambda 2$ criterion is preferred to Q criterion since the latter may be incorrect when vortices are subjected to a strong external strain [54], as it happens in our study.

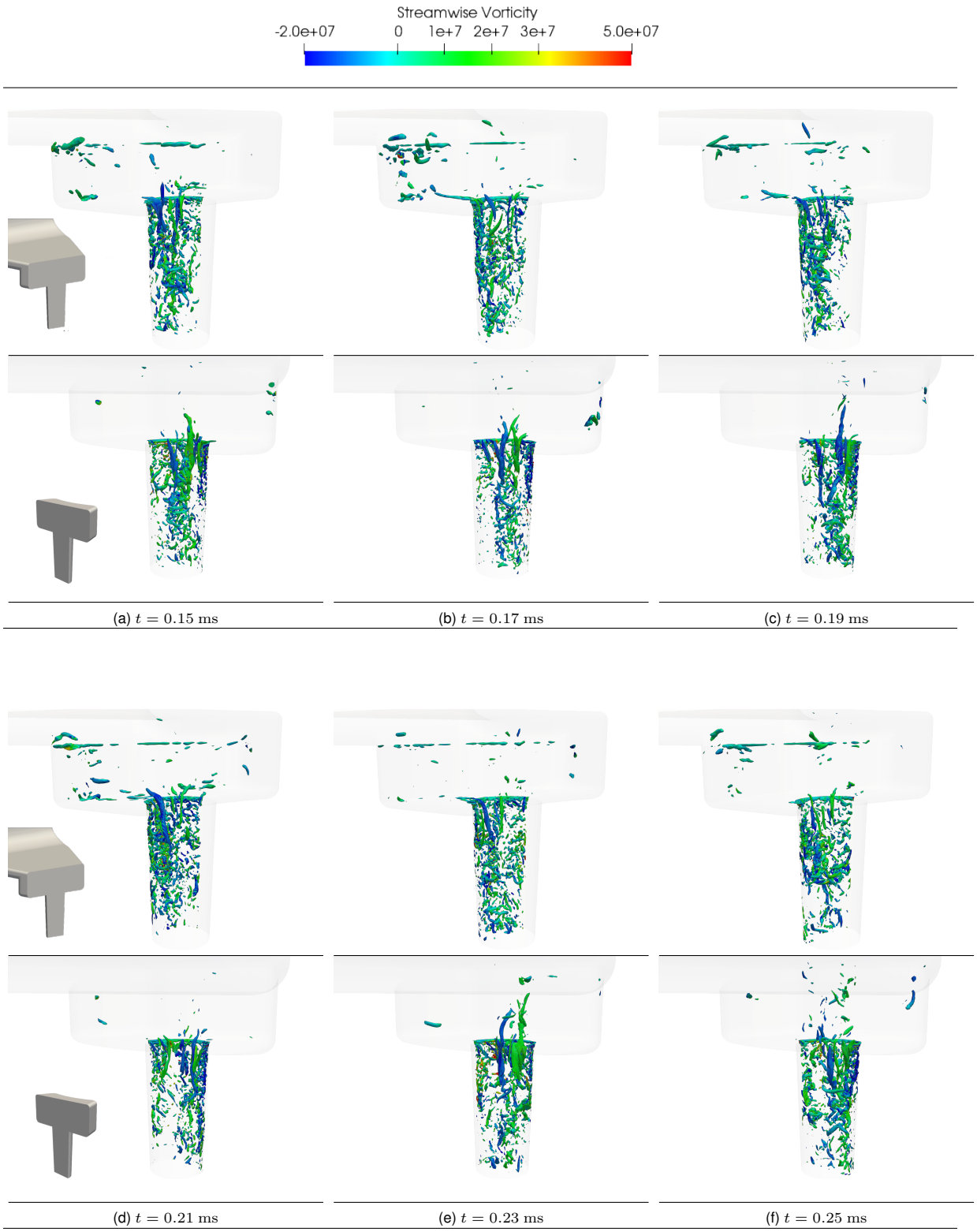

(a) $t = 0.15$ ms (b) $t = 0.17$ ms (c) $t = 0.19$ ms

(d) $t = 0.21$ ms (e) $t = 0.23$ ms (f) $t = 0.25$ ms

Figure 5. Time evolution of isosurface of λ_2 criterion coloured with streamwise vorticity for the **configuration 3**. At each istant of time the first row represents the left side view while the second row the right side view. The direction is specified by the arrow in the sketch of the geometry at bottom left

Right Section side of the nozzle in Figs. 5 and 6 shows the presence of two counter-rotating vortices in streamwise direction. Different rotation is denoted by different value of streamwise vorticity: blue structures are clockwise vortices, while green structures are anticlockwise vortices. As said previously, these structures are more accentuated

in the shortest configuration, and in Figs. 6a, 6b, 6c, they touch the upper part of the sac. On the contrary, on the left side view, smaller counter-rotating structures are bending from the sac into the nozzle, in the detached-vena zone. This zone is caracterized by the formation of hairpin vortices, which are denoted by the horizontal structures with about zero value of streamwise vorticity; They are in fact developing in the spanwise direction and in the cross (normal) direction to the flow. Thus, it must be remarked how streamwise vorticity generation is important to promote higer cavitation and higher atomization. This is what it has also been found out by other authors [55] in non-cavitating jets. In our case, streamwise vorticity growth is not only rensposible in appearance of three-dimensional instabilites but it is also promoting the onset of cavitation.

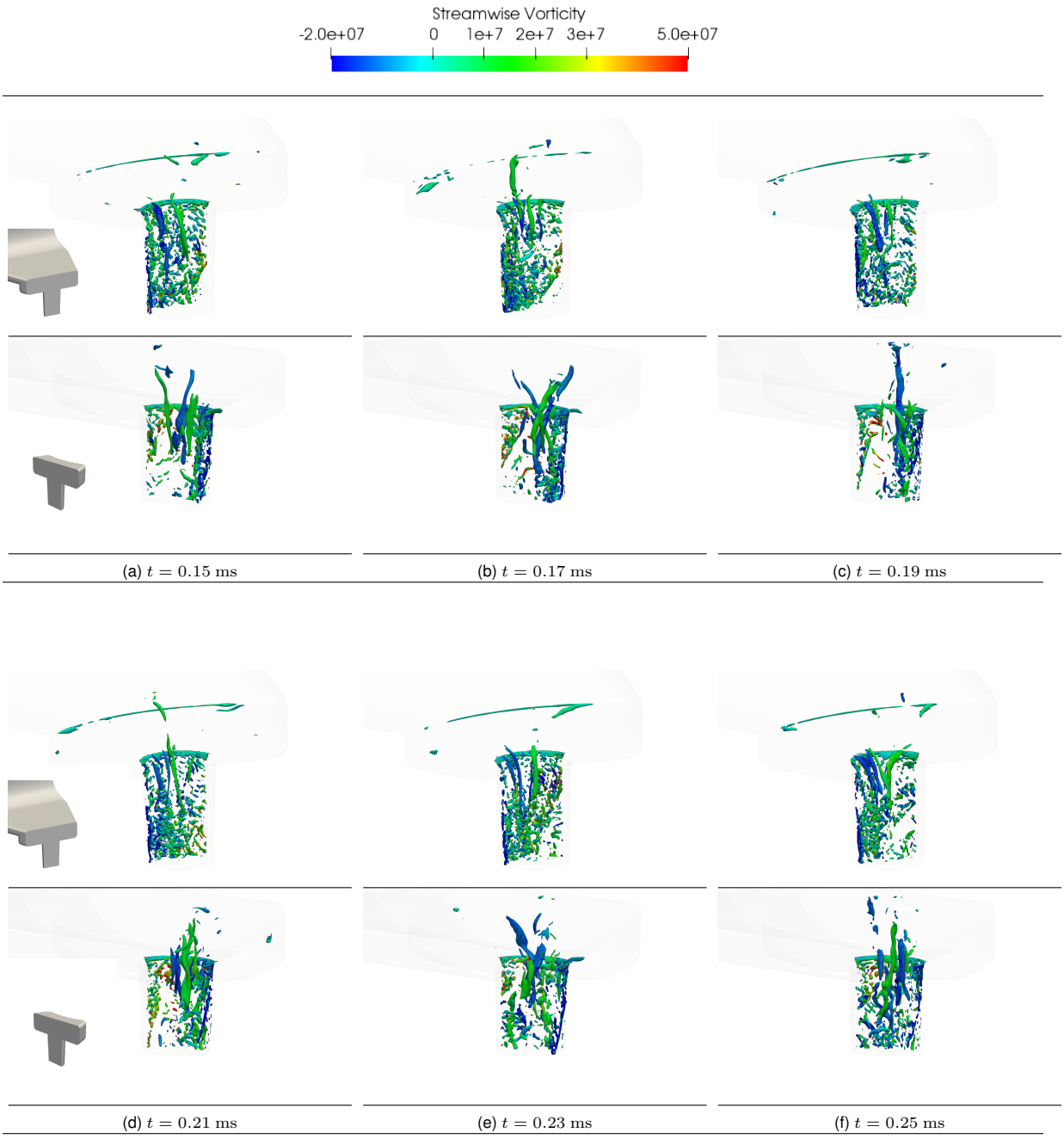

(a) $t = 0.15$ ms (b) $t = 0.17$ ms (c) $t = 0.19$ ms

(d) $t = 0.21$ ms (e) $t = 0.23$ ms (f) $t = 0.25$ ms

Figure 6. Time evolution of the isosurface of λ_2 criterion coloured with streamwise vorticity for the **configuration 10**. At each istant of time the first row represents the left side view while the second row the right side view. The direction is specified by the arrow in the sketch of the geometry at bottom left

Conclusions

The aim of the presented study was to illustrate the recently developed three-phase VOF pressure based solver, with the ability to track the air/vapour interface and model phase-change phenomena as well. The solver has been tested on two different glass nozzles. Simulations has been performed for an injection pressure of 100 bar on the nominal geometries. The aim of the simulation was to prove the predictive capability on real internal nozzle-

flow conditions and the consequent jet atomization, which is confirmed by the good agreement of experimental and numerical results in terms of average spray width and angles. Analysis of vorticity, inside the nozzles, has been performed using the $\lambda 2$ criterion. It has demonstrated how different geometries can lead to two different flow conditions and different streamwise vortices generation, which in the end is the responsible for different amount of vapour produced in the nozzle.

Acknowledgements
Authors gratefully acknowledge the Laboratory Computing Resource Center (LCRC) at Argonne National Laboratory (Lemont, US) for granting access to their HPC resources through the KNL-OPENFOAM-VOF project and the GENCI (Grand Equipement National de Calcul Intensif, France) for granting access to CINES.

References

[1] A. J. Reynolds, "Thermo-fluid dynamic theory of two-phase flow. by m. i SHIL . eyrolles 1975. 248 pp. 83f or $21.60." *Journal of Fluid Mechanics*, vol. 78, no. 03, p. 638, dec 1976. [Online]. Available: https://doi.org/10.1017/s0022112076212656

[2] C. Hirt and B. Nichols, "Volume of fluid (vof) method for the dynamics of free boundaries," *Journal of Computational Physics*, vol. 39, no. 1, pp. 201 – 225, 1981.

[3] J. A. Sethian and P. Smereka, "Level set methods for fluid interfaces," *Annual Review of Fluid Mechanics*, vol. 35, no. 1, pp. 341–372, 2003. [Online]. Available: https://doi.org/10.1146/annurev.fluid.35.101101.161105

[4] M. Sussman and E. G. Puckett, "A coupled level set and volume-of-fluid method for computing 3d and axisymmetric incompressible two-phase flows," *Journal of Computational Physics*, vol. 162, no. 2, pp. 301 – 337, 2000. [Online]. Available: http://www.sciencedirect.com/science/article/pii/S0021999100965379

[5] T. Ménard, S. Tanguy, and A. Berlemont, "Coupling level set/vof/ghost fluid methods: Validation and application to 3d simulation of the primary break-up of a liquid jet," *International Journal of Multiphase Flow*, vol. 33, no. 5, pp. 510 – 524, 2007. [Online]. Available: http://www.sciencedirect.com/science/article/pii/S0301932206001832

[6] Z. Wang, J. Yang, B. Koo, and F. Stern, "A coupled level set and volume-of-fluid method for sharp interface simulation of plunging breaking waves," *International Journal of Multiphase Flow*, vol. 35, no. 3, pp. 227 – 246, 2009. [Online]. Available: http://www.sciencedirect.com/science/article/pii/S0301932208001833

[7] M.-G. Mithun, P. Koukouvinis, and M. Gavaises, "Numerical simulation of cavitation and atomization using a fully compressible three-phase model," *Phys. Rev. Fluids*, vol. 3, p. 064304, Jun 2018. [Online]. Available: https://link.aps.org/doi/10.1103/PhysRevFluids.3.064304

[8] Y. Wang and R. D. Reitz, "Eulerian two-phase flow cfd simulation using a compressible and equilibrium eight-equation model," in *ILASS 2015, 27th Annual Conference on Liquid Atomization and Spray Systems, Raleigh,NC*, 2015.

[9] R. Saurel, F. Petitpas, and R. Abgrall, "Modelling phase transition in metastable liquids: application to cavitating and flashing flows," *Journal of Fluid Mechanics*, vol. 607, p. 313–350, 2008.

[10] F. Orley, T. Trummler, S. Hickel, M. S. Mihatsch, S. J. Schmidt, and N. A. Adams, "Large-eddy simulation of cavitating nozzle flow and primary jet break-up," *Physics of Fluids*, vol. 27, no. 8, p. 086101, 2015. [Online]. Available: https://aip.scitation.org/doi/abs/10.1063/1.4928701

[11] W. Edelbauer, "Numerical simulation of cavitating injector flow and liquid spray break-up by combination of eulerian–eulerian and volume-of-fluid methods," *Computers & Fluids*, vol. 144, pp. 19 – 33, 2017. [Online]. Available: http://www.sciencedirect.com/science/article/pii/S0045793016303747

[12] M.-G. Mithun, P. Koukouvinis, and M. Gavaises, "Numerical simulation of cavitation and atomization using a fully compressible three-phase model," *Phys. Rev. Fluids*, vol. 3, p. 064304, Jun 2018. [Online]. Available: https://link.aps.org/doi/10.1103/PhysRevFluids.3.064304

[13] S. Quan, J. Lou, and D. Schmidt, "Modeling Merging and Breakup in the Moving Mesh Interface Tracking Method for Multiphase Flow Simulations," *Journal of Computational Physics*, vol. 228, 2009.

[14] M. Altimira and L. Fuchs, "Numerical investigation of throttle flow under cavitating conditions," *International Journal of Multiphase Flow*, vol. 75, pp. 124 – 136, 2015. [Online]. Available: http://www.sciencedirect.com/science/article/pii/S0301932215001238

[15] Z. X. He, Z. Shao, Z. W. Zhou, and X. C. Tao, "Experimental study of hydraulic flip phenomenon inside diesel nozzles using diesel and biodiesel," in *Advances in Manufacturing Science and Engineering V*, ser. Advanced Materials Research, vol. 945. Trans Tech Publications, 7 2014, pp. 940–943.

[16] C. Soteriou, R. Andrews, and M. Smith, "Direct injection diesel sprays and the effect of cavitation and hydraulic flip on atomization," in *SAE Technical Paper*. SAE Int., 02 1995. [Online]. Available: http://doi.org/10.4271/950080

[17] ——, "Further studies of cavitation and atomization in diesel injection," in *International Fuels & Lubricants Meeting & Exposition*. SAE International, may 1999. [Online]. Available: https://doi.org/10.4271/1999-01-1486

[18] A. Sou, S. Hosokawa, and A. Tomiyama, "Effects of cavitation in a nozzle on liquid jet atomization," *International Journal of Heat and Mass Transfer*, vol. 50, no. 17, pp. 3575 – 3582, 2007. [Online]. Available: http://www.sciencedirect.com/science/article/pii/S0017931007001019

[19] H. Yu, L. Goldsworthy, P. Brandner, and V. Garaniya, "Development of a compressible multiphase cavitation approach for diesel spray modelling," *Applied Mathematical Modelling*, vol. 45, pp. 705 – 727, 2017. [Online]. Available: http://www.sciencedirect.com/science/article/pii/S0307904X17300410

[20] M. Cailloux, J. Helie, J. Reveillon, and F. X. Demoulin, "Large eddy simulation of a cavitating multiphase flow

for liquid injection," *Journal of Physics: Conference Series*, vol. 656, p. 012081, dec 2015. [Online]. Available: https://doi.org/10.1088/1742-6596/656/1/012081

[21] R. F. Kunz, D. A. Boger, D. R. Stinebring, T. S. Chyczewski, J. W. Lindau, H. J. Gibeling, S. Venkateswaran, and T. Govindan, "A preconditioned navier–stokes method for two-phase flows with application to cavitation prediction," *Computers & Fluids*, vol. 29, no. 8, pp. 849 – 875, 2000.

[22] J. Sauer and G. H. Schnerr, "Unsteady cavitating flow: A new cavitation model based on modified front capturing method and bubble dynamics," New York, 2000 2000.

[23] W. Yuan and G. H. Schnerr, "Numerical simulation of two-phase flow in injection nozzles: Interaction of cavitation and external jet formation," *Journal of Fluids Engineering*, vol. 125, no. 6, pp. 963–969, 2004. [Online]. Available: http://dx.doi.org/10.1115/1.1625687

[24] H. Liu, W. Zhang, M. Jia, Y. Yan, and Y. He, "An improved method for coupling the in-nozzle cavitation with multi-fluid-quasi-vof model for diesel spray," *Computers & Fluids*, vol. 177, pp. 20 – 32, 2018. [Online]. Available: http://www.sciencedirect.com/science/article/pii/S0045793018306947

[25] The OpenFOAM Foundation, "OpenFOAM User Guide." [Online]. Available: https://cfd.direct/openfoam/user-guide

[26] R. Issa, "Solution of the implicitly discretised fluid flow equations by operator-splitting," *Journal of Computational Physics*, vol. 62, no. 1, pp. 40 – 65, 1986. [Online]. Available: http://www.sciencedirect.com/science/article/pii/0021999186900999

[27] H. Weller, "A new approach to VOF-based interface capturing methods for incompressible and compressible flow," OpenCFD Ltd., Technical Report TR/HGW/04, 2008.

[28] *Large Eddy Simulation for Incompressible Flows*. Springer-Verlag, 2006. [Online]. Available: https://doi.org/10.1007/b137536

[29] S. Pope, *Turbulent Flows*. Cambridge University Press, 2000.

[30] M. Lesieur, O. Metais, and P. Comte, *Large-Eddy Simulations of Turbulence*. Cambridge University Press, 2005. [Online]. Available: https://doi.org/10.1017/cbo9780511755507

[31] X. Hu and N. Adams, "Scale separation for implicit large eddy simulation," *Journal of Computational Physics*, vol. 230, no. 19, pp. 7240 – 7249, 2011. [Online]. Available: http://www.sciencedirect.com/science/article/pii/S0021999111003342

[32] B. Knaepen, O. Debliquy, and D. Carati, "Large-eddy simulation without filter," *Journal of Computational Physics*, vol. 205, no. 1, pp. 98 – 107, 2005. [Online]. Available: http://www.sciencedirect.com/science/article/pii/S0021999104004590

[33] M. Gavaises, F. Villa, P. Koukouvinis, M. Marengo, and J.-P. Franc, "Visualisation and les simulation of cavitation cloud formation and collapse in an axisymmetric geometry," *International Journal of Multiphase Flow*, vol. 68, pp. 14 – 26, 2015. [Online]. Available: http://www.sciencedirect.com/science/article/pii/S0301932214001700

[34] R. E. Bensow and G. Bark, "Implicit LES predictions of the cavitating flow on a propeller," *Journal of Fluids Engineering*, vol. 132, no. 4, p. 041302, 2010. [Online]. Available: https://doi.org/10.1115/1.4001342

[35] X. Luo, B. Ji, X. Peng, H. Xu, and M. Nishi, "Numerical simulation of cavity shedding from a three-dimensional twisted hydrofoil and induced pressure fluctuation by large-eddy simulation," *Journal of Fluids Engineering*, vol. 134, no. 4, p. 041202, 2012. [Online]. Available: https://doi.org/10.1115/1.4006416

[36] Y. Chen, X. Chen, J. Li, Z. Gong, and C. Lu, "Large eddy simulation and investigation on the flow structure of the cascading cavitation shedding regime around 3d twisted hydrofoil," *Ocean Engineering*, vol. 129, pp. 1 – 19, 2017. [Online]. Available: http://www.sciencedirect.com/science/article/pii/S0029801816305121

[37] B. Huang, Y. Zhao, and G. Wang, "Large eddy simulation of turbulent vortex-cavitation interactions in transient sheet/cloud cavitating flows," *Computers & Fluids*, vol. 92, pp. 113 – 124, 2014. [Online]. Available: http://www.sciencedirect.com/science/article/pii/S0045793013005161

[38] B. Ji, X. Luo, R. E. Arndt, X. Peng, and Y. Wu, "Large eddy simulation and theoretical investigations of the transient cavitating vortical flow structure around a naca66 hydrofoil," *International Journal of Multiphase Flow*, vol. 68, pp. 121 – 134, 2015. [Online]. Available: http://www.sciencedirect.com/science/article/pii/S0301932214001967

[39] J. Reboud, B. Stutz, and O. Coutier, "Two-phase flow structure of cavitation:experiments and modelling of unsteady effects," in *3rd International Symposium on Cavitation, april 1998, Grenoble, France*, 1998.

[40] O. Coutier-Delgosha, R. Fortes-Patella, and J. L. Reboud, "Evaluation of the turbulence model influence on the numerical simulations of unsteady cavitation," *Journal of Fluids Engineering*, vol. 125, no. 1, p. 38, 2003. [Online]. Available: https://doi.org/10.1115/1.1524584

[41] B. Huang, A. Ducoin, and Y. L. Young, "Physical and numerical investigation of cavitating flows around a pitching hydrofoil," *Physics of Fluids*, vol. 25, no. 10, p. 102109, 2013. [Online]. Available: https://doi.org/10.1063/1.4825156

[42] B. Huang, Y. L. Young, G. Wang, and W. Shyy, "Combined experimental and computational investigation of unsteady structure of sheet/cloud cavitation," *Journal of Fluids Engineering*, vol. 135, no. 7, p. 071301, may 2013. [Online]. Available: https://doi.org/10.1115/1.4023650

[43] Y. Long, X. ping Long, B. Ji, W. xin Huai, and Z. dong Qian, "Verification and validation of urans simulations of the turbulent cavitating flow around the hydrofoil," *Journal of Hydrodynamics, Ser. B*, vol. 29, no. 4, pp. 610 – 620, 2017. [Online]. Available: http://www.sciencedirect.com/science/article/pii/S1001605816607746

[44] F. Nicoud and F. Ducros, "Subgrid-Scale Stress Modelling Based on the Square of the Velocity Gradient Tensor," *Flow, Turbulence and Combustion*, vol. 62, pp. pp. 183–200, 1999.

[45] Z. Chen, Z. He, W. Shang, L. Duan, H. Zhou, G. Guo, and W. Guan, "Experimental study on the effect of nozzle geometry on string cavitation in real-size optical diesel nozzles and spray characteristics," *Fuel*, vol. 232, pp. 562 – 571, 2018. [Online]. Available: http://www.sciencedirect.com/science/article/pii/S0016236118309670
[46] C. Hirt and B. Nichols, "Volume of fluid (vof) method for the dynamics of free boundaries," *Journal of Computational Physics*, vol. 39, no. 1, pp. 201 – 225, 1981.
[47] D. Spalding, "A method for computing steady and unsteady flows possessing discontinuities of density," CHAM Report 910/2, 1974.
[48] G. H. Schnerr and J. Sauer, "Physical and Numerical Modeling of Unsteady Cavitation Dynamics," in *ICMF-2001, 4th International Conference on Multiphase Flow*, May 2001.
[49] W. T.-F. Section and H. G. Weller, "The development of a new flame area combustion model using conditional averaging," 1993.
[50] J. Brackbill, D. Kothe, and C. Zemach, "A continuum method for modeling surface tension," *Journal of Computational Physics*, vol. 100, no. 2, pp. 335 – 354, 1992. [Online]. Available: http://www.sciencedirect.com/science/article/pii/002199919290240Y
[51] C. Brennen, *Cavitation and Bubble Dynamics*, ser. Cavitation and Bubble Dynamics. Cambridge University Press, 2013. [Online]. Available: https://books.google.it/books?id=yRhaAQAAQBAJ
[52] F. Piscaglia, F. Giussani, A. Montorfano, J. Hélie, and S. Aithal, "A multiphase dynamic-vof solver to model primary jet atomization and cavitation inside high-pressure fuel injectors in openfoam," *Acta Astronautica*, 2018.
[53] F. Giussani, A. Montorfano, F. Piscaglia, A. Onorati, J. Hélie, and S. Aithal, "Dynamic vof modelling of the internal flow in gdi fuel injectors," *Energy Procedia*, vol. 101, no. Supplement C, pp. 574 – 581, 2016, aTI 2016 - 71st Conference of the Italian Thermal Machines Engineering Association.
[54] J. Jeong and F. Hussain, "On the identification of a vortex," *Journal of Fluid Mechanics*, vol. 285, p. 69–94, 1995.
[55] A. Zandian, W. A. Sirignano, and F. Hussain, "Understanding liquid-jet atomization cascades via vortex dynamics," *Journal of Fluid Mechanics*, vol. 843, p. 293–354, 2018.